REPORT DOCUMENTATION PAGE

Form Approved
OMB NO. 0704-0188

1. AGENCY USE ONLY (Leave Blank)	2. REPORT DATE	3. REPORT TYPE AND DATES COVERED
	March 31, 1999	Final Technical Report

4. TITLE AND SUBTITLE
University Research Initiative for Rotorcraft Engine Unsteady Aerodynamics

5. FUNDING NUMBERS
ARO Grant DAAL03-92-G-0119

6. AUTHOR(S)
Sanford Fleeter

7. PERFORMING ORGANIZATION NAME(S) AND ADDRESS(ES)
Purdue Universtiy
School of Mechanical Engineering
West Lafayette, Indiana 47907

8. PERFORMING ORGANIZATION REPORT NUMBER

9. SPONSORING / MONITORING AGENCY NAME(S) AND ADDRESS(ES)
U. S. Army Research Office
P.O. Box 12211
Research Triangle Park, NC 27709-2211

10. SPONSORING / MONITORING AGENCY REPORT NUMBER
ARO 30342.1-EG-UR1

11. SUPPLEMENTARY NOTES
The views, opinions and/or findings contained in this report are those of the author(s) and should not be construed as an official Department of the Army position, policy or decision, unless so designated by the documentation.

12 a. DISTRIBUTION / AVAILABILITY STATEMENT
Approved for public release; distribution unlimited.

12 b. DISTRIBUTION CODE

13. ABSTRACT (Maximum 200 words)

Two problems driven by unsteady flow phenomena critical to advanced rotorcraft engines are addressed. (1) The surge line must be extended to higher pressure ratios. (2) Blade rows are susceptible to flow induced vibrations.

The onset and control of instability in low- and high-speed centrifugal compressors was addressed. Low speed experiments obtained unique detailed flow field data during a stall event. Also, both passive dynamic and active control techniques for the suppression of rotating stall were investigated.

A unique facility representative of a high speed, high pressure ratio centrifugal compressor was developed in cooperation with Allison Gas Turbines. Experiments were then performed to characterize the surge initiation process, including transient operation and passive control.

Experiments addressed the combined and simultaneous motion and gust induced unsteady aerodynamic response of compressor rotor blades from both flutter and forced response perspectives. Also, PIV was used to obtain a time-history of the velocity field over a chordwise bending oscillating cascaded airfoil at design and off-design. Models were developed to analyze the unsteady flow, including separatation, through an oscillating cascade and also the feasibility of active suppression of nonlinear stall flutter using piezoelectric actuators, including limit cycle, chaotic and quasi-periodic separated flow induced vibrations.

14. SUBJECT TERM	15. NUMBER OF PAGES
Instability, Rotating Stall Control, Flow Induced Vibrations, High Cycle Fatigue	24
	16. PRICE CODE

17. SECURITY CLASSIFICATION OR REPORT	18. SECURITY CLASSIFICATION ON THIS PAGE	19. SECURITY CLASSIFICATION OF ABSTRACT	20. LIMITATION OF ABSTRACT
UNCLASSIFIED	UNCLASSIFIED	UNCLASSIFIED	UL

University Research Initiative for Rotorcraft Engine Unsteady Aerodynamics

ARO Grant DAAL03-92-G-0119

Final Technical Report

May 1998

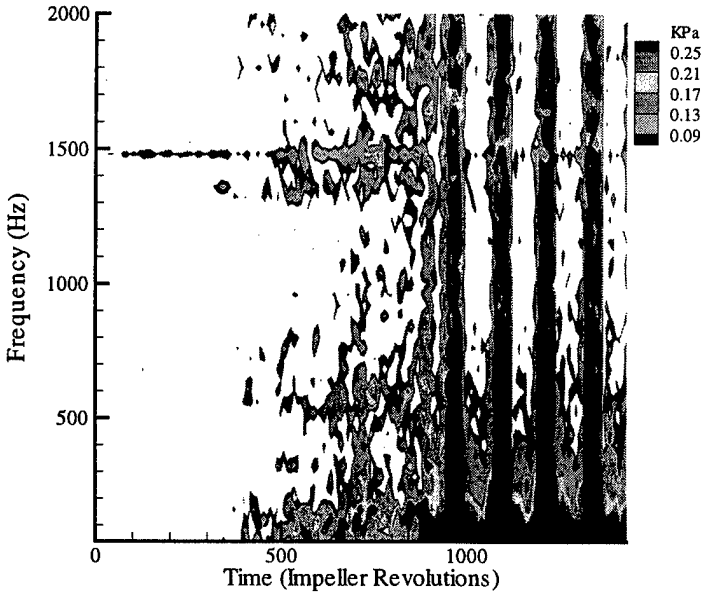

Sanford Fleeter

School of Mechanical Engineering
Purdue University
West Lafayette, Indiana 47907-1288

Table of Contents

1. Statement of the problem studied

This research is directed at two problems driven by unsteady flow phenomena critical to the development of advanced rotorcraft engines. (1) To develop high efficiency, high-pressure ratio compressors, the surge line must be extended to higher pressure ratios and compressor performance improved. (2) Rotorcraft engine axial compressors and turbines feature closely spaced low aspect ratio blade rows susceptible to significant flow induced vibrations, many of which are unique.

2. Summary of the most important results

Results: Centrifugal Compressor Rotating Stall & Surge

2.1 Low Speed

2.1.1 Purdue Low Speed Centrifugal Research Compressor: The Purdue Low Speed Centrifugal Research Compressor features a shrouded mixed flow impeller with 23 backswept blades and a diffuser which may be configured with up to 30 cambered vanes. The compressor is driven by a 29.8 kW (40HP) induction motor. The nominal operating speed for the impeller is 1,790 rpm, giving an impeller pass frequency of 29.8 Hz and a blade pass frequency of 686.2 Hz.

The compressor flow path is shown in Figure 1. Flow enters the compressor axially, passes through the impeller, enters into a curved vaneless space and then exits into a parallel walled vaned radial diffuser. The vaned section of the diffuser discharges into a vaneless, parallel walled section which in turn empties into a large collection scroll. Flow is discharged from the scroll through a discharge pipe, with a butterfly valve driven by a gear motor located at the termination of this discharge pipe serving to throttle the compressor.

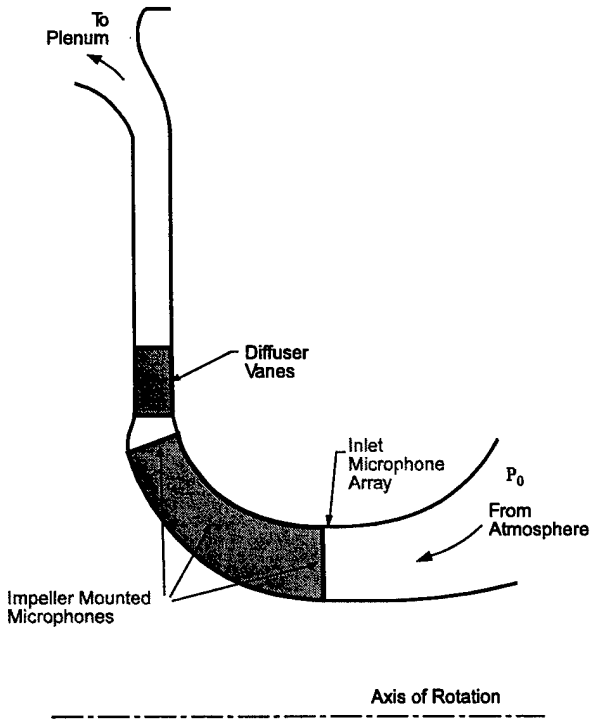

Figure 1. Low speed centrifugal research compressor flowpath

2.1.2 Rotating Stall Particle Image Velocimetry

The first centrifugal compressor Particle Image Velocimetry (PIV) measurements were successfully obtained. Namely, experiments were performed directed at obtaining unique detailed flow field data during a stall event in a low speed centrifugal compressor, with the impeller inlet and passage flow fields quantified.

To obtain these PIV impeller inlet and passage data, optical access to the impeller flow field is required. This is provided for by two plexiglass windows molded into the shroud, shown schematically in Figure 2. Each window spans one blade passage and extends approximately 50% along the blade chord. To minimize the compounding of the stress concentrations introduced by the windows, they are spaced 180° apart.

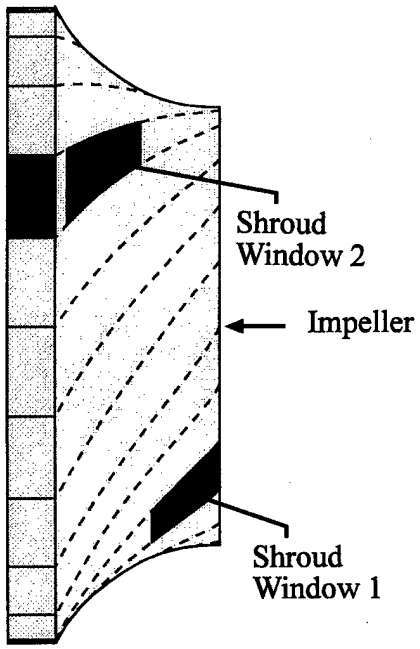

Figure 2. Impeller optical access

To obtain a deeper understanding of the rotating stall process, measurements of the flowfield itself are required. To accomplish this, PIV measurements were made in the impeller passages at a stable compressor operating point and during rotating stall. The PIV data taken during rotating stall were sorted by their position in the stall event, as identified by an inlet microphone. The microphone response was phase shifted to correspond to the center of the impeller passage during data acquisition.

One location examined is a region from 55% to 80% meridional chord. As shown in Figure 3, the light sheet intersects the suction surface at 80% span and the pressure surface at 30% span. This orientation of the light sheet was selected based on optical access and flow direction. The measurement plane closely follows the meridional streampath and avoids the suction side corner separation zone. Thus, the measurement region captures any change of the jet region characteristic of the flowpath prior to and during stall. The tangential velocity is subtracted from the total velocity. Because the measurement region is not at a constant radius, a correlation is developed for the radial location as a function of position in the measurement region.

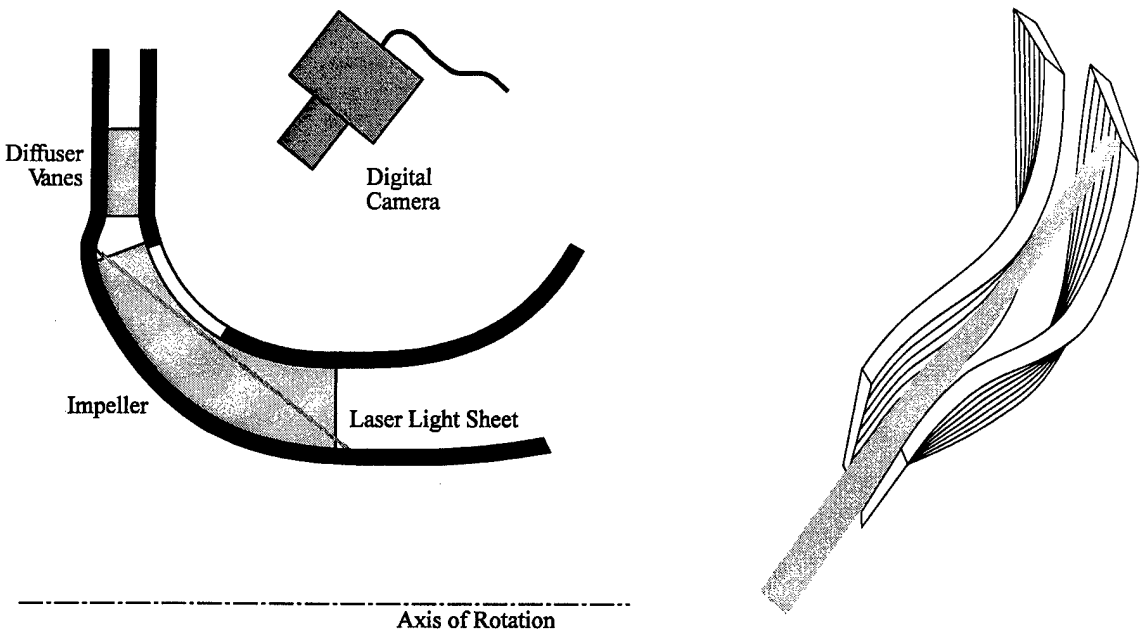

Figure 3. Flowpath cross-section of measurement plane

Velocity magnitude contours for these data are shown in Figure 4. There is significant flow acceleration above the steady flow values during the stall. This is an indication that the significant blockage associated with the stalled region is well downstream of the inducer.

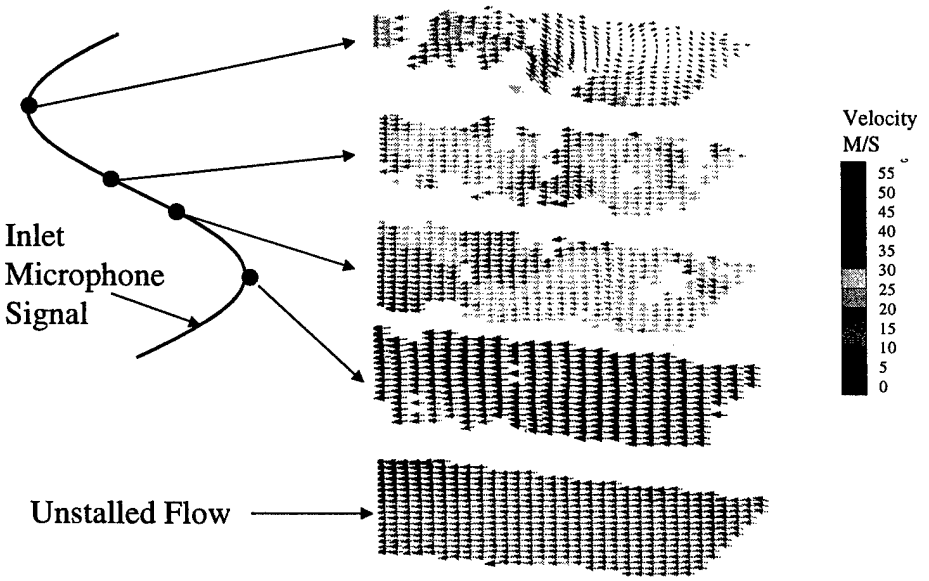

Figure 4. Impeller midchord region velocity contours during rotating stall

Stall Control: Both passive dynamic and active control techniques for the suppression of rotating stall have been investigated experimentally in the Purdue Low Speed Centrifugal Compressor. With the centrifugal compressor stall boundary controlled by the radial diffuser flow field, the passive dynamic and active control techniques are implemented in the vaned diffuser. The experiments utilize two vane configurations, 50° vane stagger and 70° vane stagger, both with 15 diffuser vanes. Primary interest is in the rotating stall event and any preceding events which may lead to the stall event. Machine performance is also of concern.

The determination of the compressor stalling point was made by observation of the standard deviation of the inlet microphone voltage. Figure 5 presents the standard deviation of the inlet microphone signal as a function of flow coefficient for nine separate stall events. The strong rise in the standard deviation is an indication of the eruption of the rotating stall in the compressor. A standard deviation of 0.25 was selected to define the stalling point for a single experiment. Variations can be observed between the stalling events, therefore it was necessary to acquire many events and average the results. Twenty throttlings were taken for each configuration. The stall point for the base diffuser configuration was 0.300 and 0.297 for the two inlets. These points are within one percent of each other and, thus, are considered identical.

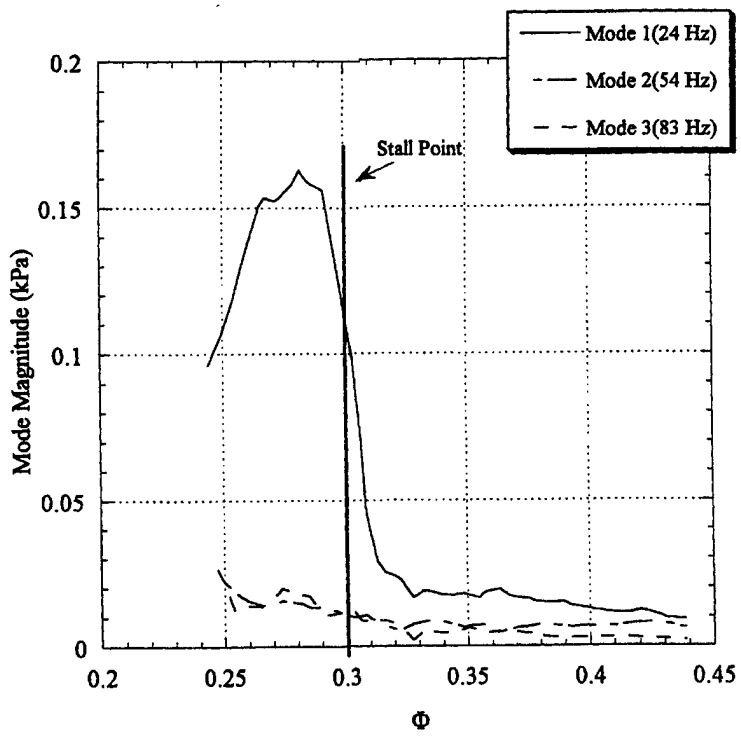

Figure 5. Mode magnitude stalling behavior for baseline 50° vane stagger

The dominant stall mode with 50° vane stagger is a one cell stall at 24 Hz. The effect of passive Helmholtz resonators, active Helmholtz resonators, and active air jets on stall initiation were investigated. Figure 6 shows these stall points depicted on a representative performance curve. The active jet control yielded a stall point of 0.294, which translates to a 2% performance range improvement. The passive independent

volume control had a stall point flow coefficient of 0.287 which is a 3.4% improvement. For the passive common volume control, a flow coefficient of 0.285 was determined to be the stall point, yielding an improvement of 4.0%. Finally, the active resonator control scheme stalled at a flow coefficient of 0.283, resulting in a 4.7% range improvement.

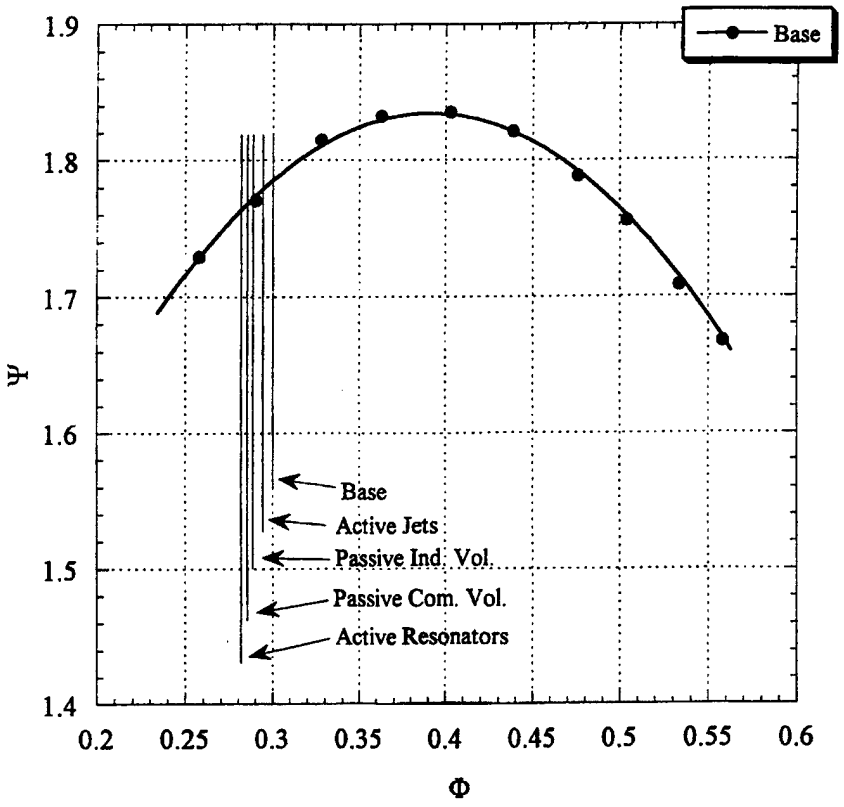

Figure 6. Stalling point comparison for 50° vane stagger

2.2 High Speed

2.2.1 Purdue High Speed Centrifugal Research Compressor Facility: To begin to provide needed high speed centrifugal compressor instability initiation information, experiments were performed directed at characterizing the surge initiation process of a high speed centrifugal compressor typical of those employed in aeropropulsion applications.

The primary components of the Purdue High Speed Centrifugal Research Compressor Facility are an Allison 250-C30G engine (C30), a slave gearbox (SG) and a centrifugal research compressor (RC), schematically depicted in Figure 7 and shown in Figure 8.

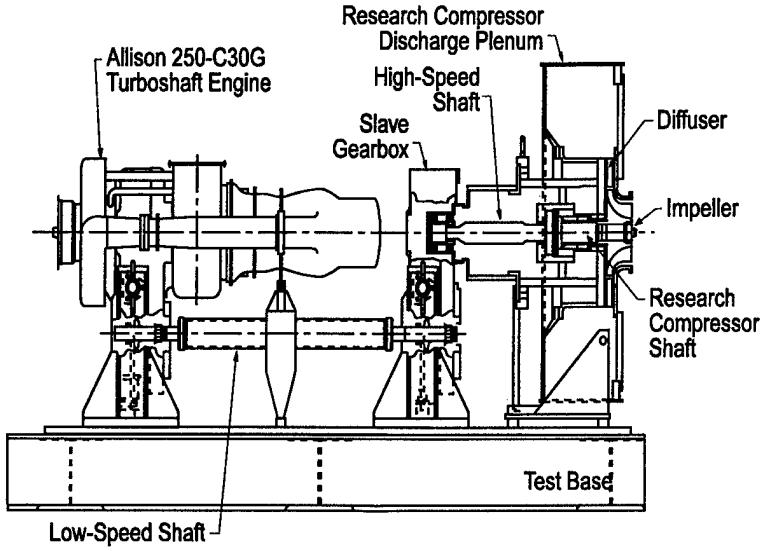

Figure 7. Purdue high speed centrifugal compressor research facility schematic

Figure 8. Purdue High Speed Centrifugal Compressor Research Facility

The C30 is a turboshaft engine producing 550 shaft Hp (415 kW). The drive engine is connected to the SGB by a low speed shaft. The slave gearbox is a highly modified unit from an Allison 250-C30G engine. A high-speed shaft connects the slave gearbox to the

research compressor. These components are individually mounted a test base in the center of the test stand.

Before entering the impeller, the air is passed through a series of screens and honeycombs to reduce the compressor inlet pressure. This both decreases the power required from the driving engine and also reduces the mechanical strain during the surge and stall experiments. After the inlet air passes through the screens and honeycomb, it enters a plenum where additional screens and honeycomb form a modified Sprenkle to reduce flow disturbances. At the end of the plenum, a contraction brings the air to the impeller inlet. Inlet surveys have shown that the impeller inlet flow is uniform. After the air passes through the impeller and the vaned diffuser, it discharges into the collection plenum and then exhausts out one side. The compressor is throttled by a butterfly valve driven by a gear motor in the exhaust pipe. Downstream of the valve and flow straighteners is a vortex flow meter to measure the compressor flow rate.

The compressor was designed by the Allison Engine Company and consists of a titanium impeller, a radial vaned diffuser, a discharge plenum and a bearing housing to support the compressor shaft. The centrifugal impeller has a nominal operating speed of 48,450 rpm, a maximum pressure ratio of 5.4 and a maximum mass flow rate of 5.5 lbm/sec (2.5 kg/sec). Thirty-six inducer bleed slots are spaced circumferentially around the compressor shroud 0.5 inches (1.3 cm) from the impeller leading edge. The design and performance parameters of the research compressor are presented in Table 1.

IMPELLER	
Tip Diameter, in. (cm)	8.5 (21.6)
Inlet Diameter, in. (cm)	5.6 (14.2)
Number of Blades	15 w/ splitte
Design Speed, rpm	48,450
Max. Pressure Ratio	5.4
Max. Flow Rate, lbs/s (kg/s)	5.5
DIFFUSER	
Inlet Diameter, in. (cm)	9.4 (23.9)
Exit Diameter, in. (cm)	13.6 (34.5)
Number of Vanes	22
Axial Passage Width, in. (cm)	0.55 (1.4)
PLENUM	
Outside Diameter, in. (cm)	33 (83.8)
Axial Length, in. (cm)	

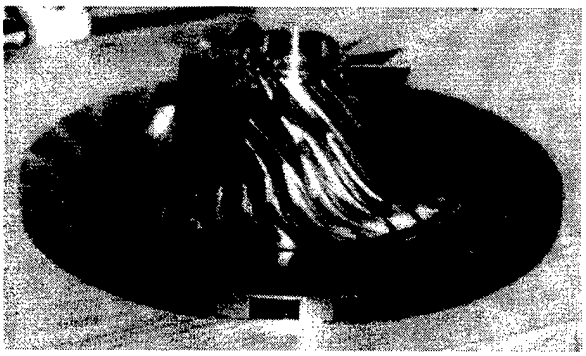

Table 1. High-speed research compressor and design performance parameters

The research compressor is extensively instrumented, as shown in Figure 9. Steady state instrumentation is utilized to determine the performance characteristics of the compressor, including the definition of the surge line. The inlet total pressure and temperature are measured in front of the inlet contraction. The exit pressure is measured by four, three element total pressure probes, with static pressure taps mounted in the endwall of the diffuser corresponding to each probe location. The stage pressure ratio is calculated by mass averaging the exit rake data. The exit temperature is measured by type K thermocouples mounted in the discharge plenum. An Endress and Hauser DSC Vortex flowmeter is used to measure the volumetric flowrate.

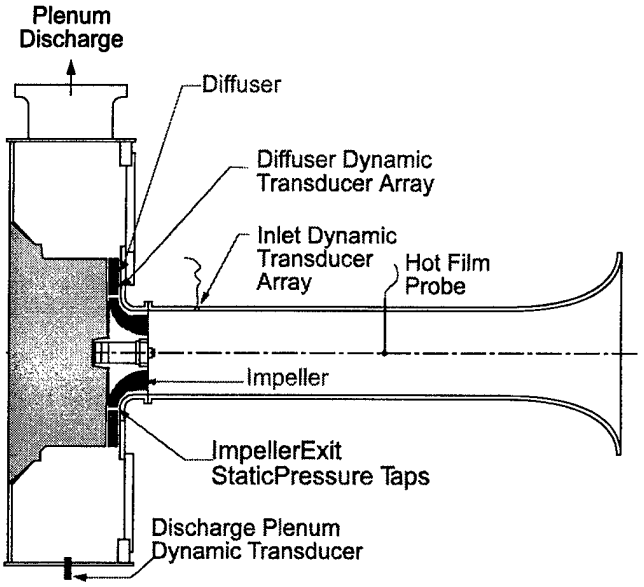

Figure 9. High speed research compressor instrumentation

An array of eight equally spaced PCB103A miniature microphones was mounted in the end wall of the impeller inlet, 3.25 inches (8.26 cm) upstream of the impeller. The transient exit static pressure is measured with a Kulite XTE-190 dynamic pressure transducer mounted in the discharge plenum opposite the plenum discharge port. An Omega PX212 dynamic pressure transducer mounted in the endwall of the inlet plenum measures the transient inlet total pressure. The instantaneous mass flow is measured using a hot-film sensor mounted in the impeller inlet section.

2.2.2 Behavior As Instability Approached

An experimental study was performed to characterize the behavior of the high speed centrifugal compressor as it approached instability. To achieve this, data at the inlet and exit of the centrifugal compressor were analyzed. Three different inducer bleed conditions are examined. Analysis of the data indicates that the disturbance was a 9 lobed stall pattern occurring in or near the diffuser, and suggests that the phenomena is different than that typically referred to as impeller stall. The component pressure characteristics show a reduction in diffuser performance corresponding to the rise in the spatial mode magnitude, with minimal effect on the impeller. It is suggested that the rotating stall condition that was observed in this compressor may play a similar role to that observed when rotating stall initiates surge in multistage axial compressor. Based on this, the investigation of non-

axisymmetric control strategies for centrifugal compression systems may be required to completely address the issue of stability control in these machines

The pressure characteristic is measured as the compressor is throttled into surge for the case of open bleed. This case was chosen because the disturbance magnitude is the largest. Figure 10 shows the impeller performance, Ψ_1, and the diffuser performance, Ψ_3-Ψ_2 as the compressor is throttled, with a trace of the first mode magnitude. At ϕ=0.52 the spatial mode magnitude begins to increase and the slope of the diffuser performance is reduced significantly. The impeller performance is not significantly affected by the rise in the spatial mode magnitude. The reduction in diffuser pressure recovery indicates that the propagating disturbance is located in the diffuser section of the compressor, rather than the impeller. The diffuser performance will result in a change in the slope of the overall characteristic, and therefore affect the stability of the compressor.

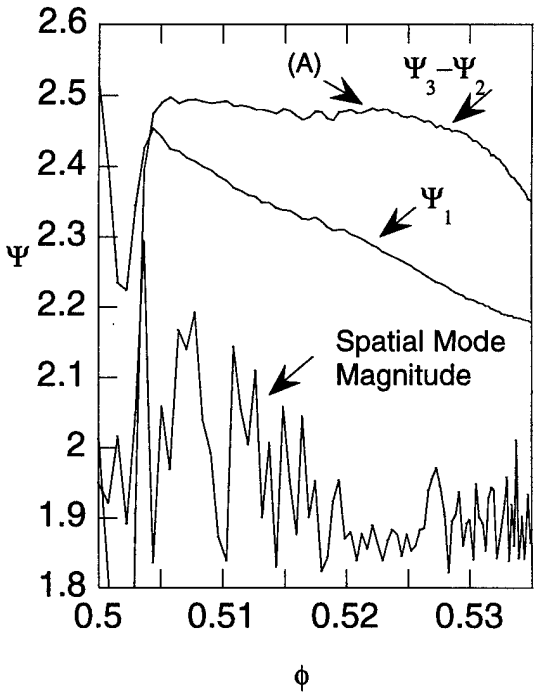

Figure 10. Diffuser and impeller performance prior to surge

2.2.3 Passive Surge Control

To determine the effects of passive surge control systems, the research compressor's diffuser has been modified. Because build clearances are so critical to compressor performance, a diffuser was designed which allows the passive control system to be disabled remotely, without disassembly of the compressor itself. In the modified diffuser, slots are machined in the endwall near the throat of the diffuser as illustrated in Figure 11.

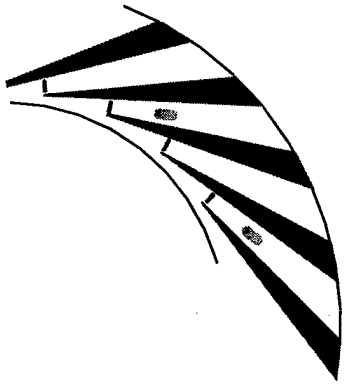

Figure 11. Instrumented diffuser

These slots serve as openings to tubes connected to the diffuser endwall that open to a common chamber, Figure 12. In this manner, the throats are connected via this chamber. The surge chamber mechanism is fitted with a series of pneumatic actuators that either allow the chamber to be open to the diffuser throats or closed off. Because the actuators are activated remotely, back to back measurements may be obtained with minimal variation of parameter other than the surge chamber.

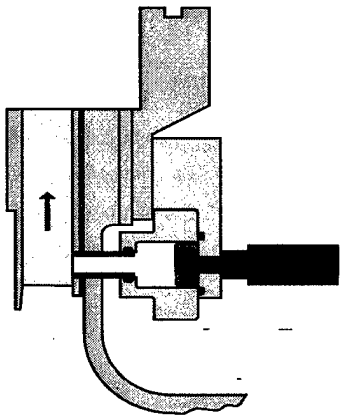

Figure 12. Surge chamber diffuser

2.2.4 Transient Operation

Quasi-steady instability initiation studies, i.e., slowly throttling the compressor into instability, are important to the understanding of the stalling behavior, and have allowed basic characteristics of compressor stability to be characterized. However, they do not model the actual operation a compressor in an installed engine. Namely, gas turbine engine compressors are subject to transient operation, with both speed and flowrate varying. During these transients, the performance of the compressor can deviate from predicted steady-state

performance, thereby reducing the effective surge margin. Figure 13 illustrates the effect of an acceleration of the compressor moving toward the surge line. Due to the inertia of the fluid in the impeller blade passages, the transient performance of the compressor deviates from the steady state operating line and moves toward the surge line.

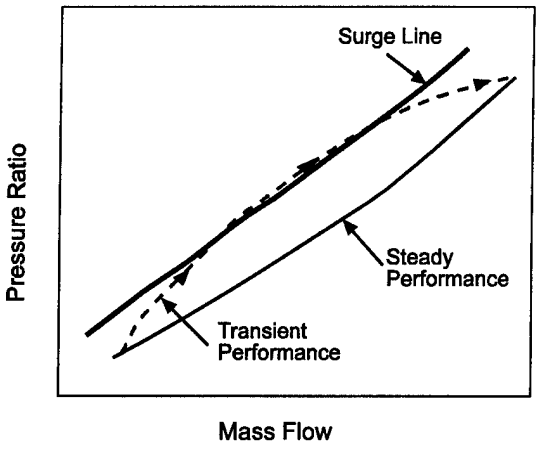

Figure 13. Transient Compressor Performance

Unfortunately, there is a dearth of high-speed centrifugal compressor instability initiation information addressing transient operation. To begin to provide this needed information, experiments are performed directed at characterizing the surge initiation process of the high-speed centrifugal compressor. Data from the high response dynamic pressure transducers installed in inlet and exit plenum are acquired as the compressor is accelerated and decelerated between full power and idle at various throttle settings. Both time-frequency spectral and transient performance measurements are employed to characterize the instability signature.

Accelerations with Baseline Diffuser: Figure 14 shows the joint time-frequency analysis performed on an acceleration from idle to full power with the compressor backpressure valve 75% closed. A discrete frequency disturbance can be seen at Point A prior to the first surge cycle at Point B. This disturbance was found to be the same disturbance shown in Figure 7.2 which was a 9 cell rotating stall. The 1452 Hz signal, however, is aliased into 548 Hz due to the sampling frequency of 2000 Hz. It is interesting to note that at Point C, after two surge cycle, there is a region of stable operation before the surge cycles resume at Point D. It is not known if there is a discrete disturbance between Points C and D due to the pressure signal saturating the analog-to-digital data acquisition board in this region. It is clear that the surge events ceased by examining the hot film signal during this time period.

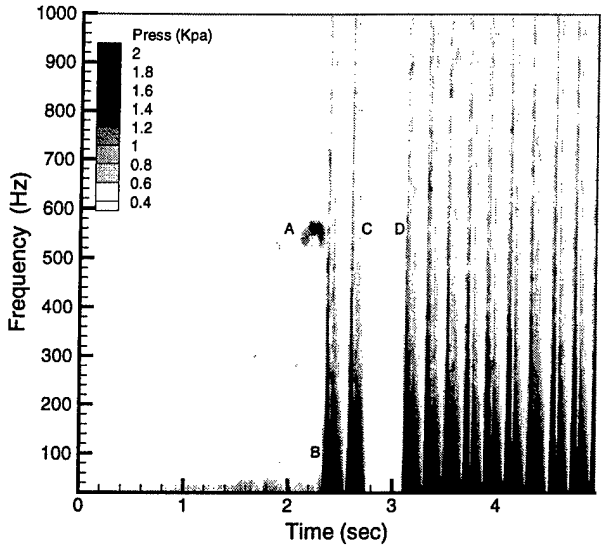

Figure 14. Joint time-frequency analysis of the plenum pressure transducer during an acceleration with throttle closed 75%

Acceleration with Complete Surge Chamber Diffuser: Figure 15 shows the joint time-frequency analysis of the plenum dynamic pressure transducer. Prior to the first surge cycle, Point M, there is a disturbance shown by Point K. Again, this is at the frequency associated with the 9 cell rotating stall. The magnitude of the disturbance is significantly reduced as compared to the baseline diffuser for a similar acceleration.

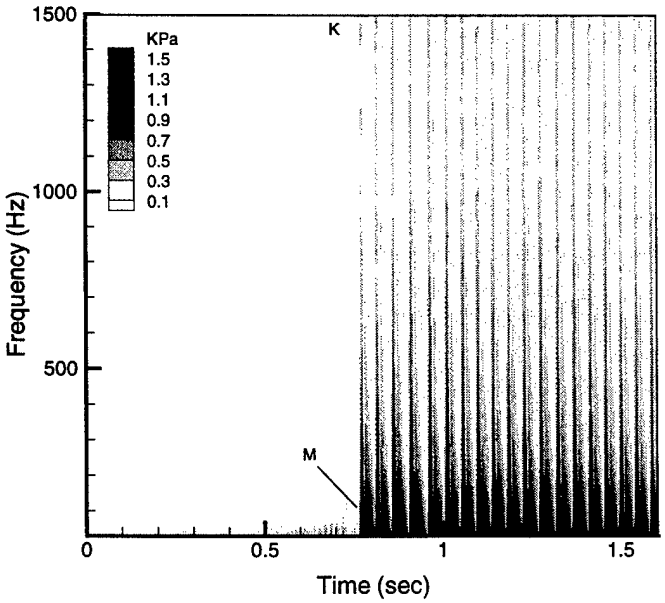

Figure 15. Joint time-frequency analysis of the plenum dynamic pressure transducer signal during an acceleration with the surge chamber diffuser

The research compressor performance is plotted in Figure 16. The research compressor's performance moves closer the steady state surge line as the pressure ratio increases. At Point N, unsteadiness brings the performance line to the surge line where deep surge initiates at Point M.

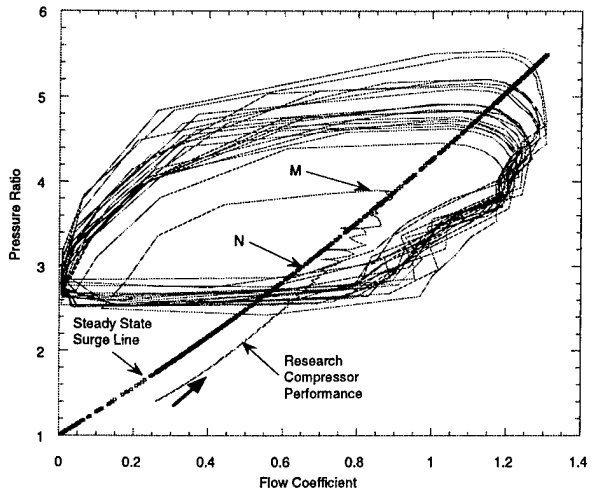

Figure 16. Transient performance during an acceleration with the surge chamber diffuser

RESULTS: FLOW INDUCED VIBRATIONS

2.3 Chordwise Bending:

Experiments were performed directed at investigating and quantifying the velocity field over a chordwise bending oscillating airfoil in a cascade operating at both design and off-design conditions. PIV was used to obtain a time-history of the velocity field over the oscillating airfoil through one complete oscillation cycle. These data were then compared with unsteady surface pressure data to identify flow phenomena responsible for the cascade unsteady aerodynamic loading distributions. High leading edge unsteady loading at zero mean incidence was attributed primarily to stagnation point migration from upper to lower surface during the oscillation cycle. The unsteadiness was enhanced by the formation of a small leading edge separation bubble which alternately grew and collapsed on the upper and lower airfoil surfaces. The reduction in leading edge unsteady loading as mean incidence increased resulted in a greatly reduced stagnation point motion which now remains on the pressure surface throughout the cycle. A substantial reduction in suction surface leading edge velocity unsteadiness was also observed. Migration of the high velocity region above the dynamic stall separation bubble resulted in increased unsteady loading between 10 and 40% chord.

Chordwise bending cascade flutter conditions were simulated by a single oscillating flat plate airfoil designed to resonate in a two-dimensional chordwise bending mode when sinusoidally excited at a frequency of 66 Hz. The airfoil was constructed from a thin stainless steel plate with shafts affixed to the hub and tip at 20 and 80 percent chord. These shafts are mounted in radial bearings in the cascade O.D. and I.D. endwalls and position the airfoil in the cascade imposing plate motion boundary conditions which produce the two-dimensional chordwise bending mode. Chordwise bending oscillations are induced by a set of four surface-bonded piezoceramic motor elements. The oscillating airfoil mounting configuration is shown in Figure 17.

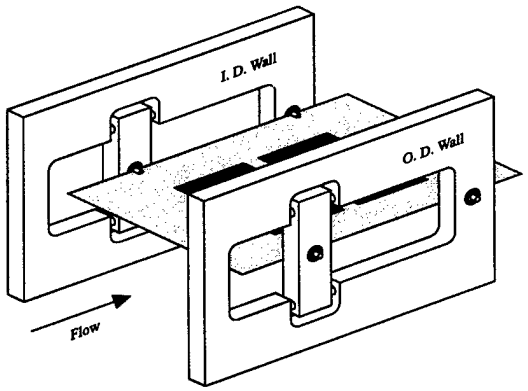

Figure 17. Chordwise bending oscillating airfoil

The PIV system configuration used to interrogate the midspan flowfield over the chordwise bending cascade airfoil is shown in Figure 18. The midspan flowfield over the chordwise bending oscillating airfoil in the Purdue Annular Cascade is illuminated by a light sheet directed axially through the test section having its plane normal to the oscillating airfoil surface. This light sheet is formed and directed to the test section by the optics train which is composed of an optical rail system mounted external to the cascade and an optical probe inserted into the cascade annulus through the O.D. endwall, 50.8 cm (20 in.) downstream of

the airfoil row trailing edge. The probe is inserted normal to the flow direction and parallel to the radial line on which the oscillating airfoil is positioned.

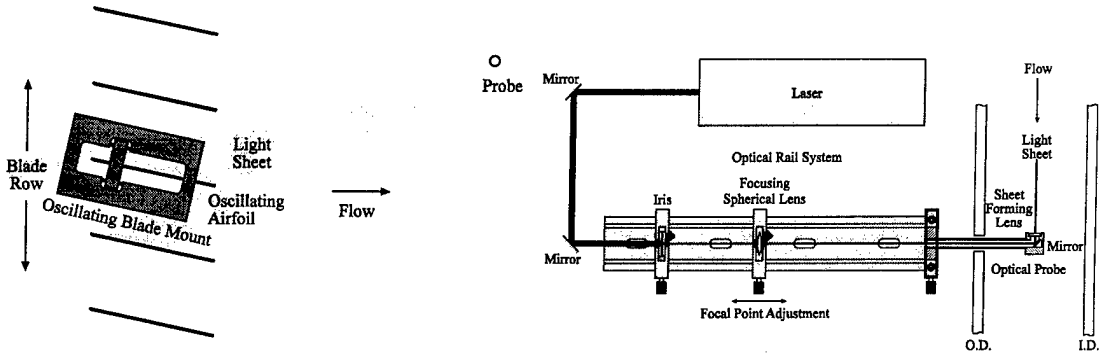

Figure 18. PIV experimental setup.

To characterize the unsteady flow over the oscillating airfoil through a complete cycle using PIV, instantaneous midspan velocity field data are obtained at a series of discrete airfoil positions. To obtain a single airfoil position velocity field in this time sequence, PIV data acquisition is triggered at a specific point in the airfoil motion cycle. The computer receives a trigger signal generated by a linear taper precision potentiometer affixed to a front mounting shaft of the oscillating airfoil. The output of this shaft potentiometer is calibrated against the airfoil leading edge midspan surface deflection. The signal thus provides the instantaneous position of the leading edge of the chordwise bending oscillating airfoil.

Figure 19 presents a time-history of the ensemble-averaged unsteady chordwise bending airfoil flowfield at 12° mean incidence.

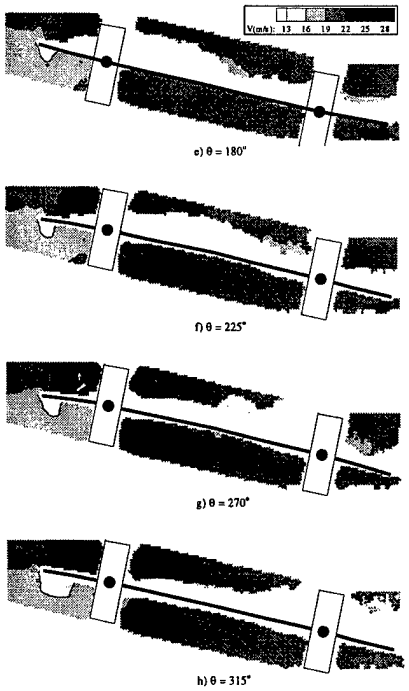

Figure 19. Ensemble-averaged unsteady flowfield at 12° mean incidence

The suction surface steady flow separation is also present throughout the oscillation cycle. However, significant dynamic effects on the size and position of the separated flow region are evident. The white regions of the suction surface velocity field where PIV images consistently failed to yield velocity data represent the ensemble-averaged position of a leading edge separation bubble and downstream vortex structures shed from that bubble. It is also consistent with the presence of strong flow acceleration over the maximum thickness region of the leading edge bubble at each airfoil position from $\theta = 0$ to 135° followed by a downstream deceleration as the flow expands into the increased flow area behind the blockage. This high velocity region moves rearward over the airfoil surface from approximately 10% chord at $\theta = 0°$ to 26% chord at $\theta = 135°$ accompanied by an apparent growth in the length of the separation bubble as the leading edge of the airfoil pitches upward through maximum deflection and begins its decent toward the mean position. At the maximum leading edge up ($\theta = 90°$) airfoil position, the data appear to capture a reattachment point behind the leading edge separation bubble.

During the second half-cycle as the airfoil leading edge pitches downward, the white region near the leading edge begins to shrink, suggesting a collapse of the separation bubble. Simultaneously, the white region downstream of the leading edge grows, possibly due to the shedding of a large vortex from the downstream edge of the bubble as it collapses. This is most evident at the $\theta = 180°$ and 225° airfoil positions where the leading edge begins to move downward decreasing flow incidence. By the time the leading edge reaches the maximum down position at $\theta = 270°$, the leading edge flow is essentially attached. Growth of a small high speed region near the leading edge between $\theta = 270°$ and 315° may be due to the early stages of formation of the separation bubble seen at $\theta = 0°$.

2.4 Combined-Simultaneous Gust & Oscillating Blade Unsteady Aerodynamics:

A detailed experimental investigation of the combined and simultaneous motion and gust induced unsteady aerodynamic response of compressor rotor blades from both flutter and forced response perspectives has been performed for the first time. The simultaneous and combined torsion motion and convected gust generated unsteady aerodynamic response of compressor rotor blades were experimentally quantified and the fundamental assumptions inherent in linear unsteady aerodynamic models addressed.

The Purdue Axial Flow Research Compressor, Figure 20, models the fundamental turbomachinery unsteady aerodynamic phenomena, including the incidence angle, the velocity and pressure variations, the reduced frequency, and the rotor and stator row geometry and flow conditions. The compressor is driven by a 15 HP DC electric motor at a speed of 2,000 RPM. The compressor has three identical stages, each containing 43 rotor blades and 31 stator vanes having a British C4 airfoil profile.

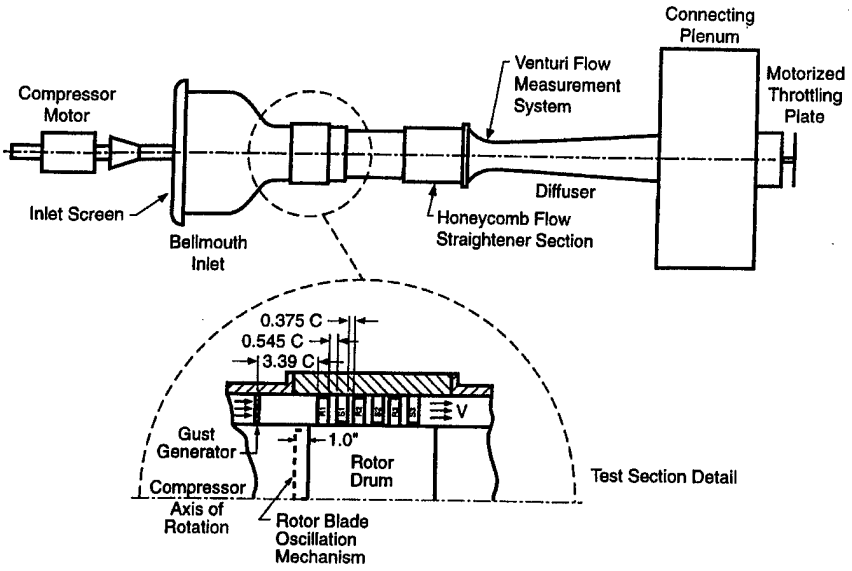

Figure 20. Purdue Axial Flow Research Compressor schematic

The rotor blade torsion mode drive system consists of three components: the blade assembly, the cam follower assembly, and the cam, Figures 21 and 22. As the compressor rotates, the cam follower rides along the sinusoidal surface of a stationary cam and its linear motion is translated into rotary motion via a lever arm fixed to the rotor blade. The elegance of this system is that the pitching motion of the rotor blades is achieved without employing any other motor drive systems - the mechanism oscillates the rotor blade as long as the compressor is operating. Also, the sinusoidal cam surface produces a single frequency harmonic motion.

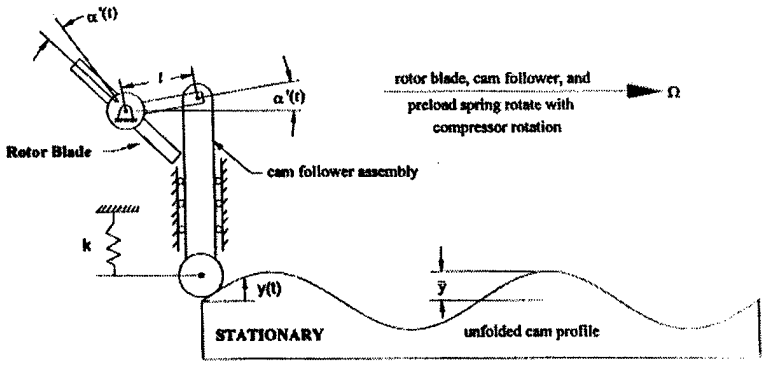

Figure 21. Rotor blade oscillation mechanism schematic

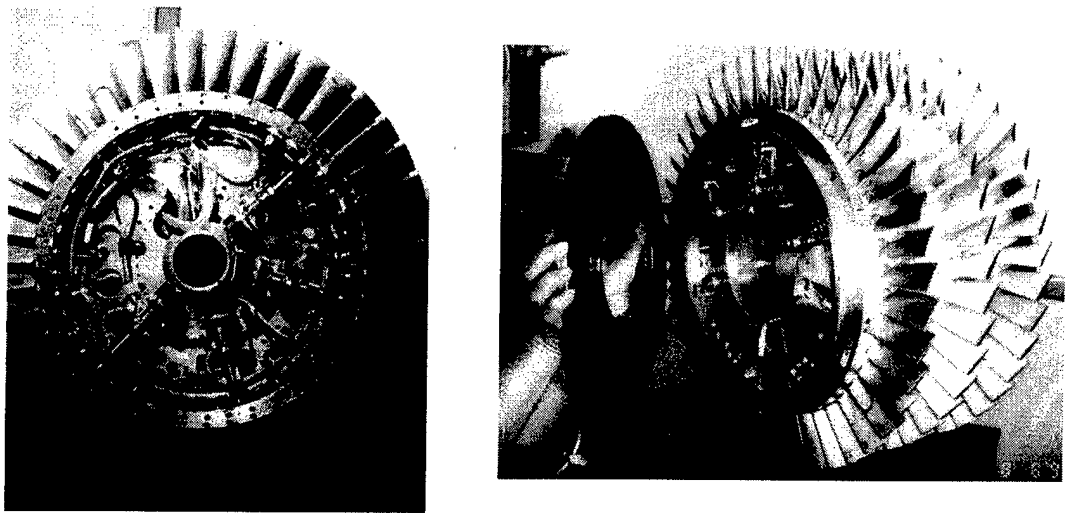

Figure 22. Rotor blade oscillation mechanism

The rotor instrumentation is shown in Figure 23. The oscillating blade motion $\alpha'(t)$ is determined by a precision rotary potentiometer whose voltage output is linearly proportional to angular position. These data are accurate to within 0.15°. The 1st stage rotor inlet flow is measured with a rotating cross hot-wire mounted at blade midspan, 18.8% chord upstream of the blade leading edge and 65.5% span circumferentially from an adjacent rotor blade. The hot-wire is calibrated for velocities ranging from 100 ft/s (30.5 m/s) to 200 ft/s (61.0 m/s) and flow angles ranging from -40° to +40°, with the velocity and flow angle uncertainty estimated to be 5% and ± 0.5° respectively.

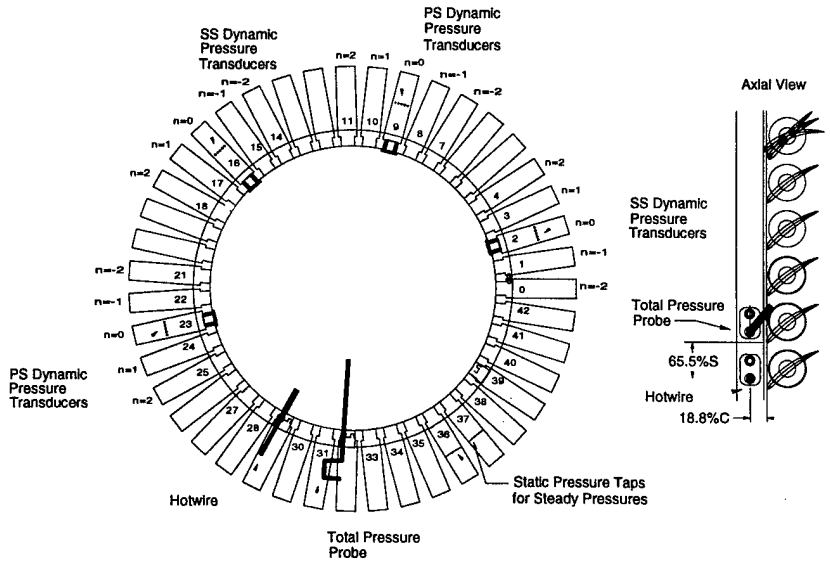

Figure 23. Rotor instrumentation

The rotor blade unsteady aerodynamics are obtained with 20 ultra miniature high response pressure transducers installed at the midspan on four blades. These transducers can operate to 10,000 g's steady and 100 g's of 2 kHz dynamic acceleration and are thus suitable for the experiment steady rotating (1018 g's) and dynamic (50 g's at 66.67 Hz) environments. The transducers were calibrated statically and dynamically.

Experiments were performed to investigate the simultaneous-combined gust and motion induced unsteady aerodynamic response of compressor 1st stage rotor blades for both forced response and flutter. The gust unsteady aerodynamics were experimentally modeled with a 2/rev forcing function to the first stage rotor blade row, generated by two perforated plates installed in the compressor inlet. The combined gust and oscillating unsteady aerodynamics were determined by the superposition of the separate oscillating blade row and gust response unsteady aerodynamics. The simultaneous gust and motion induced unsteady aerodynamic response were obtained by driving the torsion mode oscillation in the presence of the 2/Rev forcing function.

Figure 24 shows that the gust-blade motion phase should be between 20° and 180° for stability. These gust and blade motion unsteady aerodynamic effects are a direct result of the rotor incidence change caused by the interacting forcing functions. A gust-blade motion phase which results in a constructive unsteady aerodynamic interaction leads to increased unsteady lift and moment magnitudes while a destructive interaction leads to decreased magnitudes. The unsteady lift and moment phase angles are controlled by leading or lagging the gust excitation with respect to the blade motion. The gust-blade motion phase angle could be controlled by appropriately indexing the gust generators with respect to the blade motion.

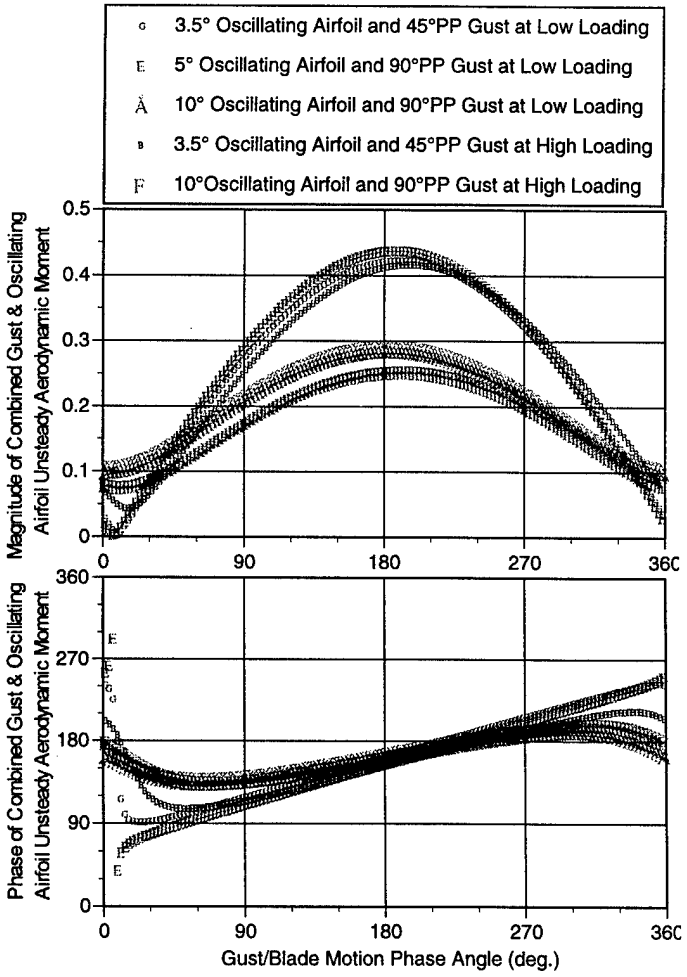

Figure 24. Gust/Blade motion phase effect on combined gust & oscillating blade moment

The combined gust and oscillating blade unsteady aerodynamic response established the applicability limits of superposition at high oscillation amplitudes and high loading, with superposition generally leading to underprediction of the unsteady lift but an overprediction of the unsteady moment. Also, the combined gust and oscillating blade unsteady aerodynamics were significantly influenced by the gust-blade motion phase angle. Gust-blade motion phase angles resulting in a constructive interaction of the gust with the oscillating blade aerodynamics increased the unsteady lift and moment magnitudes with small changes in phase. In contrast, a gust-blade motion phase angle resulting in a destructive interaction decreased the unsteady lift and moment magnitudes with large changes in phase. Thus, these results show that neglecting aerodynamic damping can lead to serious errors in forced response prediction, depending on the gust-blade motion phase angle. Also, combining a gust excitation with an oscillating blade row could alter the blade row stability, depending on the gust-blade motion phase angle.

2.5 Modeling: A mathematical model was developed to analyze the unsteady flow, including separated flow, through an harmonically oscillating cascade of airfoils. The computational model incorporates the time–marching Euler analysis, NPHASE, with an inverse integral boundary layer solution. Grid generation was simplified by utilizing an embedded composite grid formulation. Fourier series unsteady periodic boundary conditions were implemented, which reduce computational requirements. The integral turbulent boundary layer model was closed with steady correlations adopted in a quasi–steady manner. The viscous effect was modeled in the unsteady Euler solution in a quasi–steady manner by a transpiration boundary condition, thereby coupling the solution methods. An advanced design compressor geometry was utilized to study the effect of flow separation on the unsteady aerodynamics. An experimental unsteady aerodynamics data set for this configuration with separated mean flow executing torsion oscillations compared favorably with the analysis.

2.6 Friction Damper Effects On Airfoil Aeromechanics

Turbomachine design is directed at performance, accomplished with blading operating near to aeromechanics stability limits. Currently, linearized friction damper models are used to predict these stability limits. However, during engine development, these linearized solutions are often found to be inadequate. Thus, for accurate blade row stability predictions, the nonlinear effects of friction dampers must be considered. This effort was directed at investigating the effects of friction damper nonlinearities on the response of a linear system and also the applicability of linear and nonlinear aeromechanics analyses. This was accomplished utilizing both linear and nonlinear aeromechanics models to analyze a nonlinear aeromechanics system with only one nonlinearity - friction damping. The linearized friction damper results were shown to be sufficient for preliminary design and for operating conditions away from stability limits. However, nonlinear friction dampers must be considered for final design or optimization near stability limits.

2.7 Active Suppression Of Nonlinear Stall Flutter Using Piezoelectric Actuators

The feasibility of active suppression of nonlinear turbomachine blade row stall flutter, including limit cycle, chaotic and quasi-periodic separated flow induced airfoil vibrations, using piezoelectric actuators was investigated. A mathematical model was developed for the flow induced vibrations of a two degree-of-freedom intelligent airfoil driven by a nonlinear dynamic stall unsteady aerodynamic model. The control forces and moments are generated by bending and torsion piezoelectric actuators integrated into the airfoil. The resulting four dimensional model was then utilized to design the control law, accomplished based on the linearized equations of motion using the Linear Quadratic Regulator (LQR) method. Numerical results indicated that the chaotic and irregular quasi-periodic oscillations can be effectively suppressed or avoided without saturation of the piezoelectric actuator control electric field.

3. Publications & Technical Reports

Shook, P, Oaks, W., McGuire, R., Fagan, J.R. and Fleeter, S., "The Aerodynamic Performance of a High Speed Research Centrifugal Compressor Facility," *AIAA Paper 94-2798*, June 1994.

Wolff, J.M. and Fleeter, S., "Unsteady Inviscid-Viscous Analysis of Oscillating Cascade Aerodynamics," *AIAA Paper 94-2797*, June 1994.

Ehrlich, D., and Fleeter, S., "Chordwise Bending Cascade Aerodynamics by an Experimental Influence Coefficient Technique," *AIAA Paper 94-2972*, June 1994.

Kim, K and Fleeter, S., "Forcing Function Generation Fluid Dynamic Effects on Compressor Blade Gust Response," *AIAA Journal of Propulsion and Power*, Vol. 10, Number 2, March-April 1994, pp. 204-216.

Wolff, J.M. and Fleeter, S., "Single Passage Euler Analysis of Oscillating Cascade Unsteady Aerodynamics for Arbitrary Interblade Phase Angle," *AIAA Journal for Propulsion and Power*, Vol. 10, No. 5, September-October 1994, pp. 690-697.

Kim, K. and Fleeter, S., "Compressor Unsteady Aerodynamic Response to Rotating Stall and Surge Excitations," *AIAA Journal of Propulsion and Power*, Vol. 10, No. 5, September-October 1994, pp. 698-708.

Kim, K and Fleeter, S., "Compressor Blade Row Unsteady Aerodynamic Response to Attached and Separated Flow Forcing Functions," *International Journal of Turbo & Jet Engines*, Vol. 11, Nos. 2-3, 1994, pp. 201-218.

Sanders, A. and Fleeter,S., "Vane Row Indexing For Passive Vibration Control of Axial Flow Turbomachine Rotors," *AIAA Paper 95-2482*, July 1995.

Oakes, W.C., Lawless, P.B. and Fleeter, S., "Characterization of the Behavior of a Centrifugal Compressive With Active Stall Control" *AIAA Paper 95-2484*, July 1995.

Lawless, P.B., Frey, K.K., and Fleeter, S., "Rotating Stall Initiation Spatial Domain Characterization in Axial and Centrifugal Compressors," *Special Symposium on Recent Advances in Turbomachinery,* Pennsylvania State University, State College, Pennsylvania, June 1995.

Wolff, J.M. and Fleeter, S., "Nonlinear Oscillating Cascade Transonic Aerodynamic Inviscid-Viscous Analysis," *ASME Symposium on Computational Fluid Dynamics in Aeropropulsion*, November 1995.

Fleeter S, "Forcing Function Modeling For Flow Induced Vibration" 12th *International Symposium in Air Breathing Engines,* September 1995.

Sanders, A.J. and Fleeter, S., "Potential Field Interactions in a Low Speed Centrifugal Compressor," *AIAA Paper 96-2817*, July 1996.

Ehrlich, D.A. and Fleeter, S., "Incidence Effects on Chordwise Bending Cascade Unsteady Aerodynamics," *AIAA Paper 96-2667*, July 1996.

Treml, B.J. and Fleeter, S., "Passive and Active Control of Rotating Stall Onset in a Centrifugal Compressor," *AIAA Paper 96-3175*, July 1996.

Oakes, W.C., Lawless, P.B., and Fleeter, S., "High Speed Centrifugal Compressor Surge Initiation Characterization," *AIAA Paper 96-2577*, July 1996.

Li, X. and Fleeter, S., "Active Suppression of Nonlinear Stall Flutter Using Piezoelectric Actuators," *AIAA Paper 96-3177*, July 1996.

Frey, K.K. and Fleeter, S., "Oscillating Airfoil Aerodynamics of a Rotating Compressor Blade Row," *AIAA Paper 96-2673*, July 1996.

Fleeter, S., "Real Forcing Functions For Turbomachine Forced Response Analysis," *ASME Aerospace Division AD-Vol. 52*, November 1996.

Wolff, J.M and Fleeter, S., "Euler Analysis of Oscillating Cascade Aerodynamics Using Embedded Composite Grids," *International Journal of Turbo & Jet Engines*, Vol. 13, No. 3, 1996, pp. 193-210.

Li, X. and Fleeter, S., "Dynamic Stall Generated Airfoil Oscillations Including Chaotic Responses," *AIAA Paper 97-1022*, April 1997.

Markham, P.D. and Fleeter, S. "Nonlinear Aeromechanics Of Turbomachine Blading Including Friction Dampers," *ASME Paper 97-GT-111,* June 1997.

Wolff, J. and Fleeter, S., "Nonlinear Separated Inviscid-Viscous Analysis of Oscillating Cascade Aerodynamics Using an Inverse Integral Method," *ASME Paper 97-GT-85,* June 1997.

Oakes, W., Lawless, P. and Fleeter, S., "Characterization of Centrifugal Compressor Rotating Stall with Particle Image Velocimetry, *AIAA Paper 97-3282*, July 1997.

Ehrlich, D., and Fleeter, S., "Chordwise Bending Cascade Aerodynamics by an Experimental Influence Coefficient Technique," *AIAA Journal of Propulsion and Power,* January-February, 1997, pp. 39-48.

Markham, P.D. and Fleeter, S. "Nonlinear Aeromechanics Of Turbomachine Blading Including Friction Dampers," *International Journal of Turbo & Jet Engines*, Vol. 14, No. 3, 1997, pp. 173-185.

Oakes, W. Shook, P, McGuire, R., and Fleeter, S., "Aerodynamic Performance and Instability Initiation of a High Speed Research Centrifugal Compressor," *International Journal of Turbo & Jet Engines*, Vol. 14, No. 4, 1997, pp. 187-199.

Fleeter S, "Forcing Functions Generated By A High Speed Rotor Including Multi-Stage And Three Dimensional Effects," 13th *International Symposium in Air Breathing Engines,* September 1997.

Wolff, J. and Fleeter, S., "Analysis Of Nonlinear Oscillating Cascade Aerodynamics Including Separated Flow," 8th *IUTAM* International Symposium on Unsteady Aerodynamics and Aeroelasticity of Turbomachines, Stockholm, September 1997.

Frey, K.K. and Fleeter,S., "Rotating Blade Row Oscillating Airfoil Aerodynamics," 8th *IUTAM* International Symposium on Unsteady Aerodynamics and Aeroelasticity of Turbomachines, Stockholm, September 1997.

Sanders, A.J. and Fleeter, S., "Blading Response to Potential Field Interactions in Axial and Radial Flow Turbomachinery," *AIAA Journal of Propulsion and Power*, Vol. 14, No. 2, March-April 1998, pp. 199-207.

Frey, K.K. and Fleeter, S., "Rotating Compressor Blade Row Gust Unsteady Aerodynamics," *AIAA 98-3435*, July 12 - 15, 1998, Cleveland Ohio.

Oakes, W.C., Lawless, P.B. and Fleeter, S., "High Speed Centrifugal Compressor Instabilities During Speed Transients," *AIAA 98-3307,* July 12 - 15, 1998, Cleveland Ohio.

Oakes, W., Lawless, P.B., and Fleeter, S., "Characterization of Rotating Stall Behaviors in High and Low Speed Centrifugal Compressors," Herrick *International Compressor Engineering Conference at Purdue*, July 14-17, 1998.

Frey, K.K. and Fleeter, S., "Combined-Simultaneous Gust And Oscillating Compressor Blade Unsteady Aerodynamics," *ASME Paper 99-GT-*, June 1999.

Oakes, W.C., Lawless, P.B., and Fleeter, S., "Instability Pathology Of A High Speed Centrifugal Compressor," *ASME Paper 99-GT-*, June 1999.

Sanders, A.J. and Fleeter, S., "Vane Row Indexing for Passive Vibration Control of Axial-Flow Turbomachine Rotors," *AIAA Journal of Propulsion and Power*, in press.

Ehrlich, D., and Fleeter, S., "Incidence Effects on Chordwise Bending Cascade Unsteady Aerodynamics," *Journal of Propulsion and Power,* in press.

ASME Joint Propulsion Best Paper, Frey, K.K. and Fleeter, S., "Oscillating Airfoil Aerodynamics of a Rotating Compressor Blade Row," *AIAA Paper 96-2673*, July 1996.

4. Participating Scientific Personnel

James M. Wolff (Ph.D.)

Kuk Kim Frey (Ph.D.)

Brian Treml (M.S.M.E.)

Elizabeth Day (M.S.M.E.)

Patrick Markham (M.S.M.E.)

Xiao Li (Ph.D.)

Daniel Ehrlich (M.S.M.E., Ph.D.)

John Decker (M.S.M.E.)

William Oakes(Ph.D.)

Patrick Shook (M.S.M.E.)

Albert Sanders

Robert Johnston

Ron McGuire

Patrick Lawless

Sanford Fleeter